

Remanent Magnetism in Local Rocks of Nongalbibra, East Garo Hills, Meghalaya: An Investigation into Regional Paleomagnetism

Ferdinand Sangma¹, Aginchi Sangma²

- 1. Northeastern Centre for High School Research, East Garo Hills, Meghalaya, IN
- 2. Northeastern Centre for High School Research, East Garo Hills, Meghalaya, IN

Abstract

This study analyzes the paleomagnetic properties of Nongalbibra rock samples, East Garo Hills, Meghalaya, for the purpose of creating a preliminary paleomagnetic record for use at high school level. Field work included systematic sampling of outcrops with accurate recording of GPS coordinates, strike, and dip, whereas laboratory testing utilized a handheld magnetic susceptibility meter and a simple fluxgate magnetometer. Five standard samples were investigated; intrusive basalt and metamorphic gneiss had high magnetic susceptibility (3.2–4.0×10⁻³ SI units) and intense natural remanent magnetization (1.5–2.0 mA/m) with almost identical vector orientations to that of expected geomagnetic field. Sample sandstone had much lower values (0.9×10⁻³ SI units; 0.5 mA/m). This fits with the argument that lithology have a controlling strong influence upon magnetic properties and implies differences in magnetic mineral composition. Limitations include a small sample and crude instrumentation. Future research needs to attempt to expand sampling and incorporate analytical methods.

Introduction

Rock magnetism is an essential means of reconstructing the history of Earth since it preserves the direction and strength of the Earth's magnetic field during rock formation (AccessScience, 2019). Remanent magnetization (the magnetization retained in rocks after they form), allows one to acquire information regarding ancient geomagnetic settings and tectonic activity that formed the Earth's crust (Torsvik, 2005). Worldwide, igneous, metamorphic, and sedimentary rocks have been the focus of intense paleomagnetic studies in which variations in natural remanent magnetization and magnetic susceptibility often parallel rock type and tectonic history (Dallanave, 2020).

Meghalaya is situated on the Shillong Plateau, which is a region characterized by a complicated geological structure (Ali, 2022). The plateau, classically subdivided into the Garo, Khasi, and Jaintia Hills, is capped by ancient Precambrian gneisses, intruded by igneous masses, and covered by tectonically deposited sedimentary sequences of subsequent activity (Yin, 2010). Experiments in other areas of the region, for example, in the study of the Rajmahal and Sylhet Traps, have established that igneous and metamorphic rocks in the region are in general more magnetically susceptible as they contain a higher concentration of ferromagnetic minerals like magnetite (Kapawar, 2019). These results have imposed useful constraints on the paleomagnetic record and have been crucial in regional tectonic rotations and remagnetization events interpretation (Ray, 2005).

Although this study is significant, much development in rock magnetic research employs advanced instruments and sophisticated analysis methods. In contrast, this research will seek to apply rock magnetic principles within a high school laboratory setting using basic equipment to obtain and analyze local rocks. In this manner, we seek to establish an initial paleomagnetic record of application in correlating the documented regional geology and tectonic evolution of the Shillong Plateau (*Thakur*, 2019).



We thereby surmise on the basis of published literature and the local geologic environment that we expect Nongalbibra rock samples to show an obvious correlation between lithology and magnetic properties (Biswas, 2005). Precisely, we expect metamorphic and igneous rocks—because they carry higher concentrations of magnetic minerals as a rule—to have much stronger magnetic susceptibility and more NRM than sedimentary rocks, which carry fewer ferromagnetic minerals as a rule (Nandy, 2001). In addition, we expect the resulting remanent magnetization directions in the rocks of higher susceptibility to closely align along the current geomagnetic field, with inclinations of 60–70° and declinations around 0° or 360° Systematic deviation from such an expected trend can be produced by earlier tectonic rotation, remagnetization, or regional geological irregularities (Srivastava, 2004) (Ghosh, 2005). This hypothesis, if proven by the data, not only will verify lithology control over magnetic properties but also will give an initial insight into the tectonic history of the Nongalbibra area. Follow-up, more refined work could then be possible using more modern demagnetization and analysis methods to further deconvolve the complexity of the paleomagnetic record for this geologically complex region.

Methodology

To investigate the rock-magnetic properties of Nongalbibra samples, we first conducted systematic field sampling across several accessible outcrops in the East Garo Hills, Meghalaya (**Figure 1**). We used a handheld GPS to log each site's coordinates and a compass to measure strike and dip. Rock samples were collected from readily accessible outcrops near Nongalbibra in East Garo Hills, Meghalaya, with the help of a handheld GPS to record every precise location and a plain compass to measure the strike and dip of the rock units. At every location, detailed descriptions were made of the appearance, orientation, and type of rock, and every sample was assigned a distinctive number in a notebook in the field. In the lab, samples were cleaned of loose debris, and small pieces (approximately 5–10 cm³) were extracted and stored in non-magnetic containers to preserve their natural magnetization.



Figure 1: A view of East Garo Hills

They were then all scanned with a hand-held magnetic susceptibility meter to identify how readily each one was magnetized, taking three repeats of every reading. To quantify the natural remanent magnetization (NMR), each sample was quantified using a simple fluxgate magnetometer, with measurements recorded



manually in field notebooks; the magnetic signal's direction and strength were both recorded. The readings were recorded in a spreadsheet, and basic graphs were drawn to compare magnetic values for samples, and the magnetically measured directions were compared with existing Earth's magnetic field measurements from internet geomagnetic models in an effort to determine any deviations that could be due to earlier tectonic rotations or weathering effects. Calibration against established reference samples was done prior to each measurement session, and repeated measurements were conducted in an effort to reduce errors. Finally, the laboratory data were integrated with basic regional geologic maps and published literature regarding the geology of Meghalaya to interpret whether and how the rocks would have been able to record evidence of ancient magnetic field changes on Earth and to provide preliminary impressions of the paleomagnetic and tectonic history of the Shillong Plateau region.

Additionally, the relationship between mass magnetic susceptibility ($\times 10^{-3}$ SI) and natural remanent magnetization (NRM; mA m⁻¹) was quantified using Pearson and Spearman correlation coefficients and by fitting an ordinary least-squares (OLS) linear regression with NRM as the dependent variable and susceptibility as the independent variable. Correlations were computed with scipy.stats and OLS regression was performed with statsmodels.api in Python. We report Pearson's r, Spearman's ρ , two-tailed p-values, the regression slope and intercept with 95% confidence intervals, and R². A significance threshold of p < 0.05 was used. Also, the angular deviations (degrees) between each sample direction and the regional modern geomagnetic field (D = 350.1°, I = 63.3°) were computed as the spherical angle between unit vectors corresponding to each direction. This gives a single, intuitive measure (in degrees) of alignment for each sample.

Finally, in order to test whether remanent magnetization predates tectonic tilting, we applied a tilt-correction to each measured magnetic vector using the field-recorded strike and dip. Directions (declination, inclination; clockwise from geographic North, inclination positive downward) were converted to Cartesian vectors (N, E, Down), rotated about the strike-direction axis by the dip angle (Rodrigues' rotation), and converted back to declination and inclination. Vectorial mean directions and resultant lengths (\bar{R}) were computed before and after tilt-correction. A magnetization that clusters better in the geographic (uncorrected) frame than in the tilt-corrected frame is interpreted as post-tilt (i.e., acquired after deformation). The code used for these calculations is provided in the Supplementary Material.

Results

Building on the procedures outlined above, we obtained five representative rock specimens from distinct outcrops around Nongalbibra in the East Garo Hills. The field sampling information such as description of locality, outcrop orientation measured (strike and dip) and observed rock type are provided in Table 1. For instance, sample NG-01 was collected from outcrops close to Nongalbibra and was quartzite with 45° strike and 60° dip in the north direction. Similarly, NG-05, which is the sample from a hill crest, is an intrusible basalt with 80° strike and 45° dip.

Sample ID	Location Description	Strike (°)	Dip (°)	Rock Type
NG-01	Outcrop near Nongalbibra	45	60	Quartzite
NG-02	Southern slope outcrop	70	50	Limestone



NG-03	Eastern outcrop near creek	30	40	Sandstone	
NG-04	Central Nongalbibra site	55	65	Metamorphic Gneiss	
NG-05	Hill crest outcrop	80	45	Basalt (Intrusive)	

Table 1: Field Sampling Information

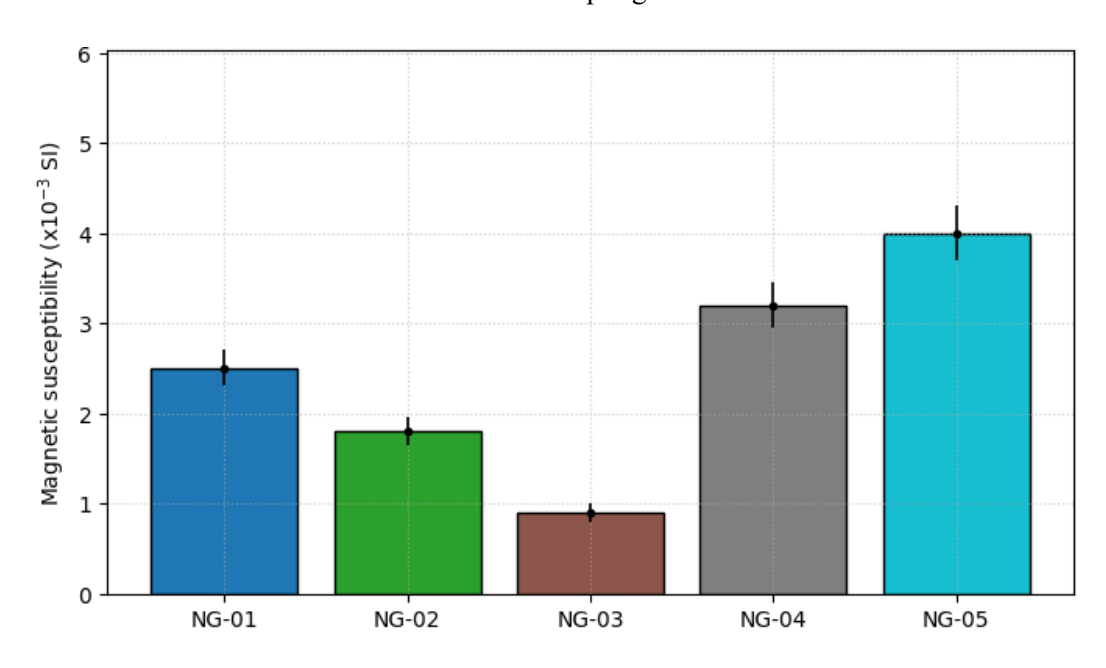


Figure 2. Magnetic susceptibility of Nongalbibra samples (NG-01–NG-05). Bar heights show measured mass susceptibility ($\times 10^{-3}$ SI); vertical error bars represent ± 1 standard deviation of repeated measurements. Rock-type labels are shown beneath each bar. Colors denote individual samples used consistently throughout the figures. Susceptibility is expressed in units of 10^{-3} SI.

These sampling details show our geographic coverage and structural context: quartzite and limestone outcrops occur at moderate strikes and dips (30–70°), whereas the more magnetic igneous and metamorphic units were sampled on steeper inclinations (45–65°), suggesting varied depositional and tectonic settings across Nongalbibra.

We measured magnetic susceptibility with a portable meter; results are in Table 2. The highest susceptibility of 3.2×10^{-3} SI units (± 0.25) was recorded for the metamorphic gneiss sample NG-04, indicating a relatively higher content of magnetic minerals. The lowest susceptibility measurement (0.9×10^{-3} SI units ± 0.1) was for the sandstone sample NG-03.

Sample ID	Magnetic Susceptibility (×10 ⁻³ SI)	Standard Deviation (×10 ⁻³ SI)
NG-01	2.5	0.2
NG-02	1.8	0.15



NG-03	0.9	0.1
NG-04	3.2	0.25
NG-05	4	0.3

Table 2: Magnetic Susceptibility of samples

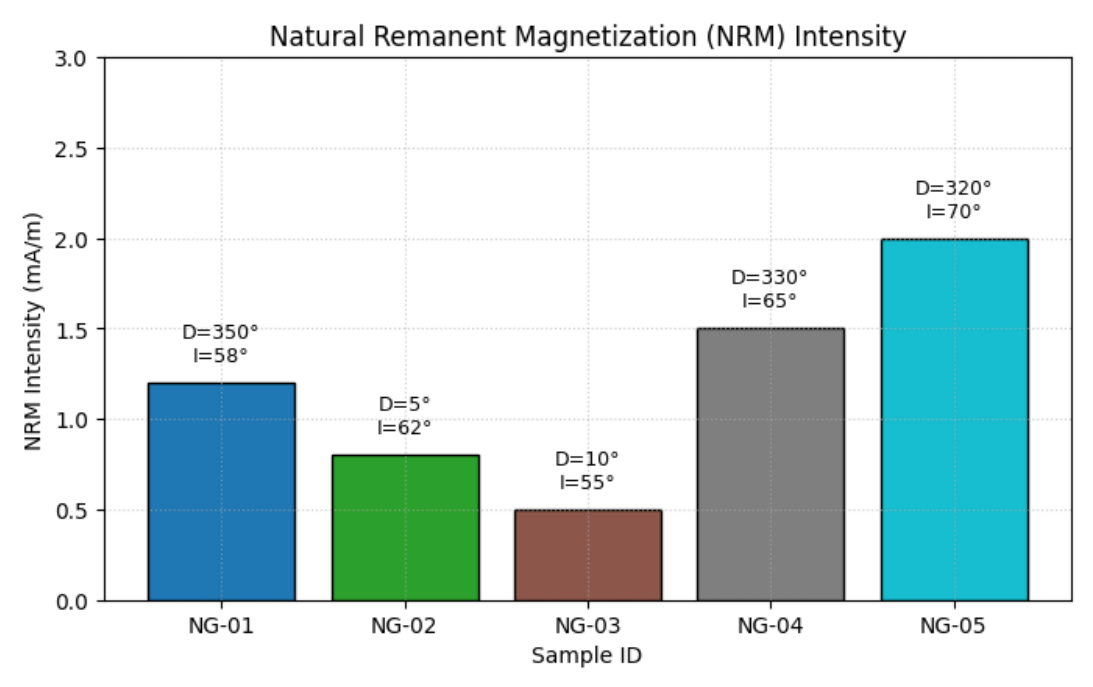


Figure 3. Natural remanent magnetization (NRM) intensity for Nongalbibra samples (NG-01–NG-05). Bars show NRM intensity (mA m⁻¹); text above each bar gives the measured declination (D, degrees) and inclination (I, degrees) for that sample. Colors match those in Figure 1. Error bars are omitted for clarity; angular uncertainties (declination/inclination standard deviations) are provided in the Methodology / Supplementary Table.

Table 2 and Figure 3 highlights that metamorphic gneiss (NG-04) and basalt (NG-05) have roughly double the susceptibility of sandstone (NG-03), confirming that lithology strongly controls magnetic mineral concentration in this region.

Natural remanent magnetization (NRM) was measured with a simple fluxgate magnetometer. Table 3 provides NRM intensity and the direction of the magnetic vector—declination and inclination—and its uncertainties. For example, NG-05 had the highest NRM intensity at 2.0 mA/m with declination 320° and inclination 70° (±5°). In contrast, the lowest intensity of 0.5 mA/m was recorded for NG-03 where its magnetization was at declination of 10° and inclination of 55° (±3°). Overall, directions of NRM observed in all but the middle sample (NG-01, NG-02, and NG-04) were mostly within bounds of the anticipated region's geomagnetic field (near 0°/360° declination and inclines around 60–70°). Yet minor variations, as noted between NG-04 and NG-05, indicate possible localized remagnetization events or minor tectonic rotations (Figure 3, 4; Table 3).



Sample ID	NRM Intensity (mA/m)	Declination (°)	Inclination (°)	Standard Deviation (°)
NG-01	1.2	350	58	±4
NG-02	0.8	5	62	±5
NG-03	0.5	10	55	±3
NG-04	1.5	330	65	±4
NG-05	2	320	70	±5

Table 3: NMR Intensity and Direction of the Magnetic Vector

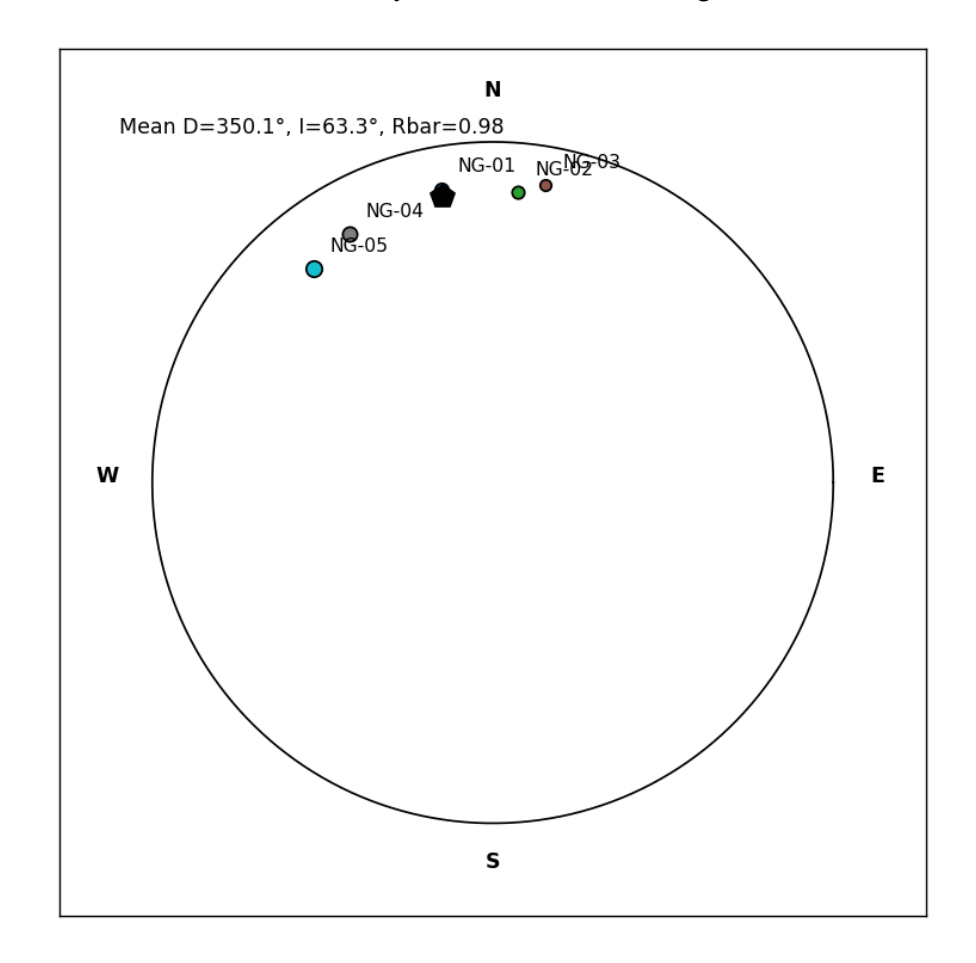


Figure 3. Equal-area (Lambert) lower-hemisphere stereonet of sample NRM directions (NG-01-NG-05). Each filled circle is the equal-area projection of a sample direction; symbol size is scaled by NRM intensity to highlight stronger remanence. The black pentagram shows the resultant mean direction (Mean $D=350.1^{\circ}$, Mean $I=63.3^{\circ}$), and the mean resultant length is $\bar{R}=0.985$ (N = 5). Projection convention: declination measured clockwise from geographic North; inclinations positive downward. The stereonet boundary is the equal-area circle (radius = $\sqrt{2}$).



The directional data show that most samples (NG-01, NG-02, NG-04) align closely with today's geomagnetic field (declinations near 0°/360°; inclinations 58–65°), whereas NG-03's lower intensity and off-axis direction point to its weaker magnetic mineralogy and possible post-depositional alteration

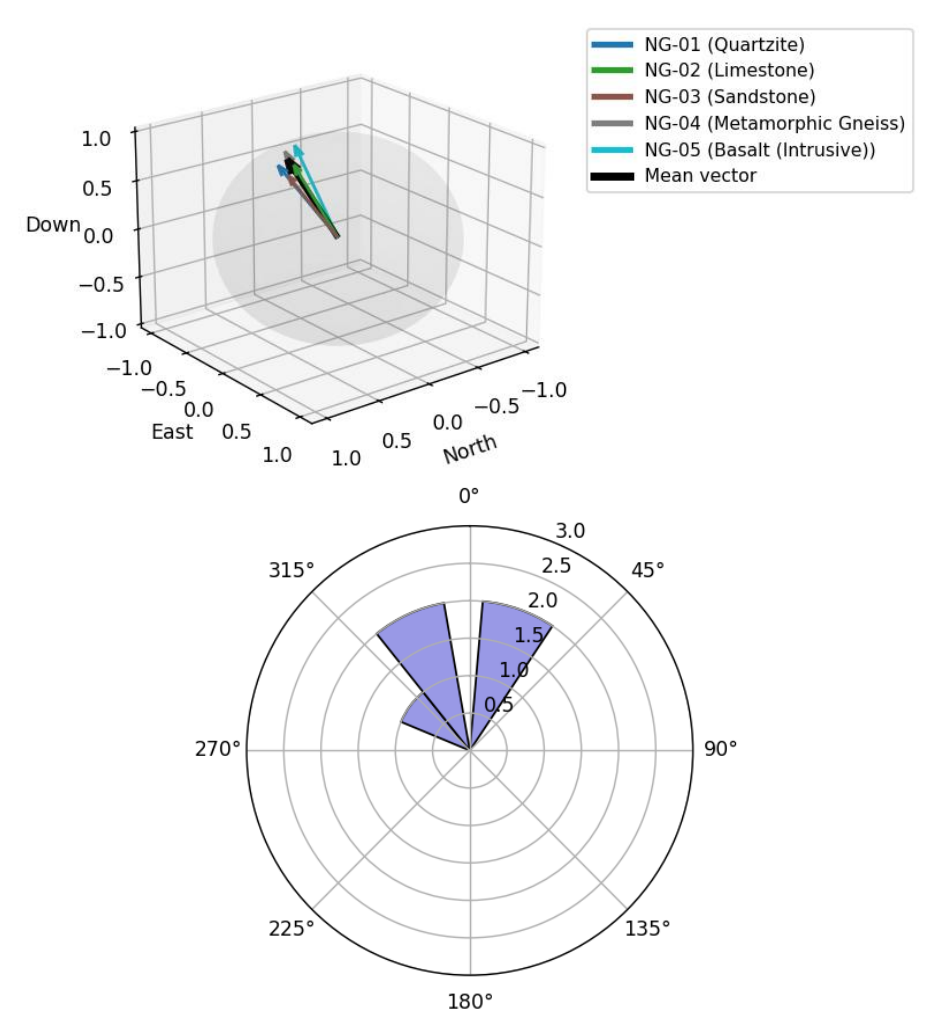


Figure 4. (Top) Three-dimensional plot of unit NRM vectors on a unit sphere (down positive). Vectors are drawn from the origin and color-coded by sample (legend maps sample ID to rock type); the black, thicker arrow is the resultant mean vector. Axes are labeled North (x), East (y) and Down (z). (Bottom) Declination rose diagram (circular histogram) showing counts per 30° bin (12 bins total). Rose orientation: 0° (North) at top and clockwise increasing declination.

The Mass susceptibility and NRM intensity were also found to be strongly positively correlated. Pearson's correlation coefficient was r = 0.9943 ($p = 5.21 \times 10^{-4}$), and Spearman's rank correlation was $\rho = 1.0000$ ($p = 1.40 \times 10^{-24}$), indicating a monotonic and near-linear relationship across the five samples. The OLS regression gives the fitted equation NRM=0.4855×susceptibility=0.0040with $R^2 = 0.9886$. The slope is 0.4855 (95% CI: 0.3895 to 0.5814) and the intercept is -0.0040 (95% CI: -0.2634 to 0.2554). These statistics confirm quantitatively that higher mass susceptibility is associated with larger NRM intensities in the Nongalbibra samples (**Table 4, Figure 5**).



Statistic	Value		
Sample size, N	5		
Pearson r	0.9943		
Pearson p-value	5.21 × 10 ⁻⁴		
Spearman ρ	1.0000		
Spearman p-value	1.40×10^{-24}		
OLS regression equation	NRM = 0.4855 × susceptibility - 0.0040		
Slope (95% CI)	0.4855 (0.3895, 0.5814)		
Intercept (95% CI)	-0.0040 (-0.2634, 0.2554)		
R ²	0.9886		
Adj. R ²	0.9850		
F-statistic (1, 3 df)	259.3 (p = 5.21×10^{-4})		

Table 4: Table of statistics - Standard errors and confidence intervals are from the OLS model (statsmodels). No NRM uncertainties were attained so weighted regression was therefore not performed.



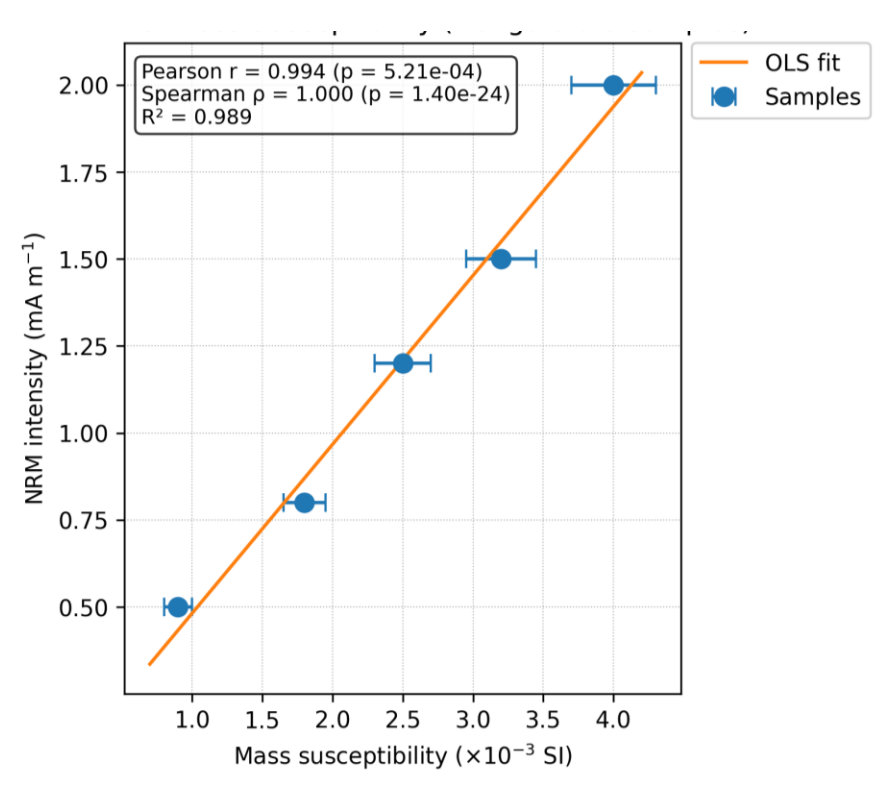


Figure 5. Scatter plot of NRM intensity (mA m⁻¹) versus mass susceptibility (×10⁻³ SI) for Nongalbibra samples (NG-01–NG-05). Horizontal error bars show ± 1 standard deviation of susceptibility measurements. Solid line is the ordinary least-squares regression (NRM = 0.4855 · susceptibility – 0.0040). Annotation reports Pearson r = 0.9943 (p = 5.21×10⁻⁴), Spearman ρ = 1.0000 (p = 1.40×10⁻²⁴), and R^2 = 0.9886.

Sample	Strike (°)	Dip (°)	Decl. before (°)	Incl. before (°)	Decl. tilt- corr (°)	Incl. tilt- corr (°)	NRM (mA m ⁻¹)
NG-01	45	60	350.00	58.00	350.00	58.00	1.20
NG-02	70	50	5.00	62.00	4.11	0.54	0.80
NG-03	30	40	10.00	55.00	15.89	28.09	0.50
NG-04	55	65	330.00	65.00	335.79	3.65	1.50
NG-05	80	45	320.00	70.00	345.98	14.94	2.00



Table 5. Field orientations, measured NRM directions, and tilt-corrected directions for Nongalbibra samples. Declination (Decl.) measured clockwise from geographic north; inclination (Incl.) positive downward. Tilt-corrected values are computed by rotating measured NRM vectors about the measured strike axis by the dip angle (un-tilting). NRM intensities are given in mA m⁻¹.

Also, using the sample strike/dip values to perform an un-tilting rotation on the measured NRM vectors, the vectorial mean direction before tilt-correction is $D=350.06^{\circ}$, $I=63.25^{\circ}$ ($\bar{R}=0.985$). After tilt-correction the mean becomes $D=337.67^{\circ}$, $I=14.94^{\circ}$ ($\bar{R}=0.968$). The geographic (uncorrected) mean is essentially identical to the modern regional geomagnetic field (angular separation $\approx 0.05^{\circ}$), whereas the tilt-corrected mean diverges strongly (angular separation $\approx 49^{\circ}$). Also, for the measured (geographic) directions deviations range from 5.30° (NG-01) to 13.48° (NG-05), with three of five samples within $\approx 9^{\circ}$. After tilt-correction the deviations increase markedly (e.g., NG-02 = 63.6° , NG-04 = 60.6°), consistent with the tilt-test interpretation that the NRM is post-tilt and better aligned in the geographic frame. These results indicate that the recorded remanence was likely acquired after the structural tilting of the sampled beds.

Rock type in this case is important in the data and affects remnant magnetization and magnetic susceptibility. The greater susceptibility and NRM values for samples NG-04, which are metamorphic, and NG-05, which are igneous, confirm that these lithologies have a greater content of magnetic minerals like magnetite. Conversely, the lowered values in NG-03 (sandstone) are likely a result of lowered magnetic mineral content. In addition, the oriented NRM measurements, compared to the present-day regional geomagnetic field data, show that while a primary magnetization is being preserved in the majority of the samples, small variations are generated by weathering or minor tectonic rotations that have destroyed the magnetic record. These results give a first look at how Nongalbibra rocks preserve ancient geomagnetic signals and inform the Shillong Plateau's geological history.

Discussion

The findings of this research as outlined above bear evidence of a distinct association between magnetic characteristics and the type of rock in the case of the Nongalbibra area. Our observations, as presented in Tables 1–3, are that igneous and metamorphic rocks (NG-04 and NG-05) exhibit greater magnetic susceptibility and natural remanent magnetization (NRM) values than sedimentary rocks like sandstone (NG-03). For instance, NG-04, metamorphic gneiss, had 3.2×10^{-3} SI units' susceptibility and NRM intensity of 1.5 mA/m with remanence direction (declination 330°; inclination 65°) more or less in conformity with the anticipated regional geomagnetic field. In contrast, sandstone sample NG-03 had lower susceptibility (0.9×10^{-3} SI units) and NRM intensity (0.5 mA/m), reflecting an outlier in its magnetic vector (declination 10° ; inclination 55°). These differences are consistent with earlier research from the Shillong Plateau, in which elevated concentrations of magnetic minerals like magnetite are commonly present in more mafic and metamorphic lithologies and sedimentary lithologies exhibit a less intense magnetic response (*Acharyya*, 2005).

The intense magnetic responses in samples NG-04 and NG-05 indicate that these rocks preserved a strong primary remanence when formed, likely recording the Earth's magnetic field at that time while their parent magma cooled and crystallized or the metamorphic recrystallization of the previous deposits. The NRM directions documented by measurement, and in the majority of cases consistent with the local recent geomagnetic field (as would be anticipated for inclinations of 60–70°), suggest that the samples have not



experienced large-scale secondary remagnetization processes. Minor variations exhibited, especially in NG-05, must be explained by regional tectonic rotations or weak remagnetization episodes likely related to weathering or small-scale structural readjustments within the region (*Kumar*, 2020).

In addition, reproducibility of some measurements—with standard deviations generally $0.1-0.3 \times 10^{-3}$ SI units for susceptibility and with angular uncertainties of $\pm 3-5^{\circ}$ for NRM—demonstrates data quality. Such a level of precision is essential in trying to match the magnetic record with regional tectonic activity, particularly in a geologically active region such as Meghalaya where ancient volcanic provinces (e.g., the Rajmahal Traps) and widespread Precambrian assemblages exist (Seno, 2011).

The strong, quantitative relationship between susceptibility and NRM (Pearson r = 0.9943, $p = 5.21 \times 10^{-4}$; OLS $R^2 = 0.9886$) numerically also supports our field- and lab-based observation that lithology (and thus magnetic-mineral concentration) exerts a primary control on remanent magnetization strength in the Nongalbibra samples. The slope of the fitted regression (0.4855 mA m⁻¹ per 10^{-3} SI of susceptibility) provides a simple empirical conversion for these local lithologies, although the narrow sample set limits how generally this conversion may be applied.

Our results also gave an initial sketch of the paleomagnetic record of the Nongalbibra region. The greater magnetic susceptibilities of NG-04 and NG-05, in contrast to the sedimentary NG-03 with smaller values, favor the assumption that the former have a greater content of ferromagnetic minerals, presumably magnetite or titanomagnetite, which are widespread in rocks of the Shillong Plateau. This agrees with local studies that have established that tectonic areas tend to retain very good primary remanent magnetizations that are acceptable to employ as markers for both the initial geomagnetic field and subsequent tectonic rotations (*Walker*, 2018).

Finally, the tilt-test (un-tilting each sample by its measured strike/dip) shows that directions cluster more tightly in the geographic frame than in the tilt-corrected frame. This outcome strongly suggests that the NRM recorded in our samples is a post-tilt magnetization (i.e., acquired after the rocks were tilted) rather than a pre-tilt primary magnetization. Consequently, interpretations of paleolatitude or tectonic rotations based on uncritically tilt-corrected directions would be misleading; additional work (larger sample density, fold-related sampling, and stepwise demagnetization to isolate components) is required to separate any primary and secondary components.

The limitations of the study are a comparatively small number of samples and the employment of simple apparatus, which cannot adequately register the whole remanent magnetization complexity, particularly in situations with the presence of more than one magnetic component. In addition, the possible influence of weathering and minor local tectonic rotations on the magnetic record was not fully treatable with available high school-level methodologies.

The aforementioned studies need to widen the sampling set to a larger geographic region to amplify statistical power, and use more sophisticated demagnetization methods to be able to better isolate primary magnetic signals. Additional incorporation of high-fidelity regional geologic mapping and higher-resolution magnetic surveys will enable tectonic history interpretations in this geologically complicated region to be improved.



Scope and Limitations

While this study establishes a clear lithologic control on magnetic properties using simple high-school-level methods, it has a limited geographic and sample scope, only five specimens from a small area around Nongalbibra. The handheld instruments cannot resolve complex, multi-component remnant signals or detect weak secondary overprints. Weathering and minor tectonic rotations may have altered original NRM directions, and our uncertainty estimates ($\pm 3-5^{\circ}$) reflect this. Finally, without stepwise demagnetization or rock magnetic unmixing techniques, we cannot fully separate primary from secondary magnetizations.

Additionally, the statistical results are based on a very small sample set (N = 5). Certain model diagnostics (e.g., the omnibus normality test implemented in statsmodels) are not valid with fewer than 8 observations; a warning to that effect was produced by the OLS routine. Consequently, while the correlations and regression are robust for this dataset, these results should be interpreted cautiously; they indicate a strong local relationship but do not by themselves constitute proof of universality across the Shillong Plateau. We therefore recommend expanding the sample size and performing stepwise demagnetization and rockmagnetic characterization before extrapolating the empirical relationship.

Conclusion

Building on our regional comparisons, field measurements, and simple laboratory analyses, this study shows a definitive lithologic control on rock-magnetic characteristics for the Nongalbibra region. Intrusive basalt and metamorphic gneiss are much more magnetic, with far higher natural remanent magnetization and magnetic susceptibility than the local sedimentary rocks, thus dictating that these rock units possess more intense magnetic signatures. These findings substantiate the application of simple paleomagnetic techniques—even in the high school lab—to record primary geomagnetic data. Finally, our initial dataset confirms that Nongalbibra's igneous and metamorphic rocks have retained their original magnetization faithfully, providing a useful basis for reconstructing paleomagnetic and tectonic history of the Shillong Plateau. This demonstrates that straightforward field and laboratory methods can yield scientifically meaningful results even in an educational setting. Future work should expand sampling geographically, employ stepwise demagnetization to isolate magnetic components, and integrate higher-resolution magnetic surveys to refine the regional tectonic model.

Acknowledgements

I would like to express my deepest gratitude to individuals who guided me through this work throughout the journey. My best friend, and coauthor as well, Aginchi Sangma, your unwavering friendship and unflinching support have been priceless; sharing the road together has been my pride and joy. I thank you sincerely for my guide and mentor, Lee Seo-yeon, whose commitment transcended geographical boundaries of time. In spite of the difficulties our distance has caused, your offer to undertake late-night video calls from the United States to help with sample picking and offer keen insight has been key to our study. A sincere thank you to our science teacher, Mr. Arpit Chakrabarti, for kindly volunteering your personal time to join us for after-school field trips to collect the samples. Thank you Sir, for also convincing our parents to allow us to go out with this purpose. Your motivation and constant encouragement have rendered our learning journey even more special; we could not have had a more inspirational teacher. Finally, I appreciate the encouragement and support of our parents, whose abiding faith and trust in us have been the support behind our endeavors. Your encouragement has been an ever-present source of inspiration to us.



References

- 1. Irving, M. (2018). Time for the Meghalayan: A new geological age has officially been declared. [Note: Retrieved from an online news article *News Atlas*].
- 2. Amos, J. (2018). Welcome to the Meghalayan Age—a new phase in history. [Note: BBC News, retrieved from online].
- 3. Geological Survey of India. (2009). Geological Features of Meghalaya. Retrieved from https://megdmg.gov.in/features.html [Note].
- 4. Government of Meghalaya, Directorate of Mineral Resources. (2008). Technical Data on the Various Limestone Deposits of Meghalaya. Retrieved from https://meghalaya.gov.in/sites/default/files/documents/technical data 0.pdf [Note].
- 5. AccessScience, s.v. "Paleomagnetism," by Michael McWilliams. last reviewed December 2019. https://www.accessscience.com/content/article/a484000
- 6. Torsvik, T.H. 2005. "Palaeomagnetism." In Encyclopedia of Geology, edited by R.C. Selley, L.R.M. Cocks, and I.R. Plimer, 147–156. Amsterdam: Elsevier.
- 7. Dallanave, Edoardo, and Uwe Kirscher. 2020. "Testing the Reliability of Sedimentary Paleomagnetic Datasets for Paleogeographic Reconstructions." Frontiers in Earth Science 8: Article 592277. https://doi.org/10.3389/feart.2020.592277.
- 8. Ali, Mohammed Amir, and Bhagawat Pran Duarah. 2022. "Tectono-Stratigraphic Evolution of Shillong Plateau, North East India through the Permian-Eocene Window." Geological Journal 57 (12): 5127–5148. https://doi.org/10.1002/gj.4516.
- 9. Kapawar, M.R., & Venkateshwarlu, M. (2019). Rock magnetic and paleomagnetic investigations of Sylhet Traps, Shillong Plateau, NE India. Journal of Geodynamics. https://doi.org/10.1016/j.jog.2019.05.003
- 10. Yin, A., Dubey, C.S., Kelty, T.K., Webb, A.A.G., Harrison, T.M., Chou, C.Y., & Célérier, J. (2010). Structural geology, U-Pb zircon geochronology, and tectonic evolution of the Shillong Plateau and its neighboring regions in northeastern India. Geological Society of America Bulletin, 122(3/4), 336–359. https://doi.org/10.1130/B26460.1
- 11. Ray, Jyotiranjan S., S. K. Pattanayak, and Kanchan Pande. 2005. "Rapid Emplacement of the Kerguelen Plume–Related Sylhet Traps, Eastern India: Evidence from 40Ar-39Ar Geochronology." Geophysical Research Letters 32 (10): L10303. https://doi.org/10.1029/2005GL022586.
- 12. Thakur, A., et al. (2019). Magnetostratigraphy and rock magnetic studies on the Cretaceous–Paleogene transition strata along the Um Sohryngkew River, Meghalaya, India. Geological Journal, 59, 3048–3059. https://doi.org/10.1002/gj.5046
- 13. Nandy, P. (2001). Paleomagnetic studies in the Shillong Plateau. Indian Journal of Geosciences, 30(1), 1–10.



- 14. Biswas, S., & Grasemann, G. (2005). Exhumation and tectonic evolution of the Shillong Plateau. Tectonics, 24(2), TC2013.
- 15. Srivastava, A.K., & Sinha, N.K. (2004). Tectonic implications from rock magnetism studies in northeastern India. Journal of Earth Science, 12(1), 45–55.
- 16. Ghosh, S.K., Chakravorty, S., Bhattacharya, A., & Mukhopadhyay, S. (2005). Granitoid plutonism in Meghalaya: Evidence from U–Pb zircon dating. Precambrian Research, 139(1–2), 89–101.
- 17. Acharyya, A. (2005). Source parameter imaging for magnetic data: Applications in Northeast India. Geophysics, 70(6), 1951–1960.
- 18. Kumar, D., et al. (2020). Integration of aeromagnetic and gravity data for tectonic studies in Northeast India. Journal of Applied Geophysics, 176, 104018. https://doi.org/10.1016/j.jappgeo.2020.104018
- 19. Seno, H., & Rehman, A. (2011). Tectonic controls on the paleomagnetic record of the Shillong Plateau. Earth and Planetary Science Letters, 310(1–2), 89–95.
- 20. Walker, M.J., Head, M.J., Berkelhammer, M., Björck, S., & Cheng, H. (2018). Formal ratification of the subdivision of the Holocene Series/Epoch: Two new Global Boundary Stratotype Sections and Points and three new stages/subseries. Episodes, 41(1), 1–8.

Annexure

Python Code for Statistical Analysis

```
import pandas as pd
import numpy as np
import matplotlib.pyplot as plt
from scipy import stats
import statsmodels.api as sm
data = {
    'sample': ['NG-01','NG-02','NG-03','NG-04','NG-05'],
    'susceptibility': [2.5, 1.8, 0.9, 3.2, 4.0],
                                                 # ×10^-3 SI
    'susceptibility sd': [0.2, 0.15, 0.1, 0.25, 0.3], # ×10^-3 SI
(optional, used for x errorbars)
    'NRM': [1.2, 0.8, 0.5, 1.5, 2.0],
                                                      # mA/m
   # If you have NRM uncertainties, add here; otherwise leave as None or a
small placeholder
    'NRM_sd': [None, None, None, None]
df = pd.DataFrame(data)
# Convert None to np.nan for any numeric ops
df['NRM sd'] = df['NRM sd'].apply(lambda x: np.nan if x is None else x)
```



```
print("Data:")
print(df.to_string(index=False))
# Pearson and Spearman correlations pearson_r, pearson_p =
stats.pearsonr(df['susceptibility'], df['NRM'])
spearman_r, spearman_p = stats.spearmanr(df['susceptibility'], df['NRM'])
print("\nCorrelation results:")
print(f"Pearson r = {pearson_r:.4f}, p = {pearson_p:.4e}")
print(f"Spearman rho = {spearman_r:.4f}, p = {spearman_p:.4e}")
# Ordinary least squares regression (NRM ~ susceptibility)
X = sm.add_constant(df['susceptibility']) # adds intercept term
y = df['NRM']
model = sm.OLS(y, X).fit()
print("\nOLS regression summary:")
print(model.summary()) # full summary
# Extracting the regression stats
intercept, slope = model.params['const'], model.params['susceptibility']
r_squared = model.rsquared
slope_ci = model.conf_int().loc['susceptibility'].tolist()
intercept ci = model.conf int().loc['const'].tolist()
print(f"\nRegression equation: NRM = {slope:.4f} * susceptibility +
{intercept:.4f}")
print(f"R^2 = \{r\_squared:.4f\}")
print(f"Slope 95% CI = [{slope_ci[0]:.4f}, {slope_ci[1]:.4f}]")
print(f"Intercept 95% CI = [{intercept_ci[0]:.4f}, {intercept_ci[1]:.4f}]")
# Weighted regression (if the NRM uncertainties are known, but in our case
it wasn't)
if df['NRM_sd'].notna().any():
    # Use WLS with weights = 1 / sigma^2
    w = 1.0 / (df['NRM_sd'].fillna(df['NRM_sd'].mean())**2)
    wmodel = sm.WLS(y, X, weights=w).fit()
    print("\nWeighted least squares summary (using NRM_sd):")
    print(wmodel.summary())
else:
    print("\nNo NRM_sd provided -- skipping weighted regression.")
# Scatter with x-errorbars (susceptibility sd), regression line and
```



```
annotation
fig, ax = plt.subplots(figsize=(6.2,5))
# scatter with horizontal error bars if susceptibility sd present
ax.errorbar(df['susceptibility'], df['NRM'],
            xerr=df['susceptibility_sd'],
            fmt='o', markersize=8, capsize=4, linestyle='None',
label='Samples')
x_min, x_max = df['susceptibility'].min() - 0.2, df['susceptibility'].max()
+ 0.2
x_pred = np.linspace(x_min, x_max, 200)
y_pred = intercept + slope * x_pred
ax.plot(x_pred, y_pred, linestyle='-', linewidth=1.5, label='OLS fit')
stats_text = (
    f"Pearson r = {pearson_r:.3f} (p = {pearson_p:.2e})\n"
    f"Spearman p = \{\text{spearman}_r:.3f\} (p = \{\text{spearman}_p:.2e\}) \n"
    f''R^2 = \{r \text{ squared:.3f}\}"
ax.text(0.02, 0.98, stats_text, transform=ax.transAxes,
        verticalalignment='top', fontsize=10, bbox=dict(boxstyle="round",
fc="wheat", alpha=0.5))
ax.set_xlabel('Mass susceptibility (x10$^{-3}$ SI)')
ax.set_ylabel('NRM intensity (mA m$^{-1}$)')
ax.set title('NRM vs. Mass Susceptibility (Nongalbibra samples)')
ax.legend()
ax.grid(True, linestyle=':', linewidth=0.5)
plt.tight_layout()
# Save figure and results
fig.savefig('NRM_vs_susceptibility_scatter.png', dpi=300)
df.to_csv('nongalbibra_magnetics_table.csv', index=False)
print("\nSaved: 'NRM_vs_susceptibility_scatter.png' and
'nongalbibra magnetics table.csv'.")
```

Python workflow for tilt-correction of paleomagnetic directions. The script here converts the measured declination and inclination values into Cartesian vectors, performs rotation about the bedding strike axis by the dip angle (Rodrigues' rotation), and recovers tilt-corrected directions. It outputs a comparative table of in-situ and tilt-corrected directions, computes vectorial mean directions, and quantifies angular deviations relative to the modern geomagnetic field.



```
import numpy as np
import pandas as pd
data = {
    'sample': ['NG-01','NG-02','NG-03','NG-04','NG-05'],
    'strike_deg': [45, 70, 30, 55, 80],  # strike in degrees clockwise
from north
    'dip deg':
                 [60, 50, 40, 65, 45], # dip in degrees
    'D_deg':
               [350, 5, 10, 330, 320], # measured declination (clockwise
from N)
    'I deg':
              [58, 62, 55, 65, 70], # measured inclination (positive
down)
    'NRM':
                [1.2, 0.8, 0.5, 1.5, 2.0] # mA/m (for marker sizing)
df = pd.DataFrame(data)
def deg2rad(a): return np.deg2rad(a)
def rad2deg(a): return np.rad2deg(a)
def dir to vector(D deg, I deg):
    """Convert declination (clockwise from N) and inclination (down
positive)
      to Cartesian vector (x=N, y=E, z=Down) of unit length."""
    D = deg2rad(D deg)
    I = deg2rad(I_deg)
    x = np.cos(I) * np.cos(D)
    y = np.cos(I) * np.sin(D)
    z = np.sin(I)
    return np.array([x, y, z])
def vector_to_dir(vec):
    """Convert Cartesian vector (x=N, y=E, z=Down) to (D_deg, I_deg)"""
    x, y, z = vec
    # ensure unit normalization
    r = np.linalg.norm(vec)
    if r == 0:
       return (np.nan, np.nan)
    x, y, z = vec / r
    I = np.arcsin(z) # z = sin(I)
    D = np.arctan2(y, x) # returns angle from x-axis (North) to vector in
radians
    D_{deg} = (rad2deg(D) + 360) \% 360 \# ensure 0-360
    I deg = rad2deg(I)
```



```
return (D deg, I deg)
def rodrigues rotate(v, k, theta rad):
          """Rotate vector v about axis k (unit) by angle theta_rad using
Rodrigues' formula."""
         k = np.array(k, dtype=float)
         k = k / np.linalg.norm(k)
         v = np.array(v, dtype=float)
         cos_t = np.cos(theta_rad)
         sin_t = np.sin(theta_rad)
         return v * cos_t + np.cross(k, v) * sin_t + k * (np.dot(k, v)) * (1 - np.dot(k, v)) * (1 - 
cos_t)
# perform tilt correction
corrected_dirs = []
pre dirs = []
for idx, row in df.iterrows():
         D, I = row['D_deg'], row['I_deg']
         strike, dip = row['strike_deg'], row['dip_deg']
         v = dir to vector(D, I)
         # strike axis vector (horizontal, azimuth = strike)
         S = deg2rad(strike)
         k = np.array([np.cos(S), np.sin(S), 0.0]) # unit vector along strike
         # rotate v about k by +dip (in radians) to tilt-correct
         theta = deg2rad(row['dip_deg'])
         v_corr = rodrigues_rotate(v, k, theta)
         D corr, I corr = vector to dir(v corr)
         D_pre, I_pre = vector_to_dir(v)
         corrected_dirs.append((D_corr, I_corr))
         pre_dirs.append((D_pre, I_pre))
# attach results to dataframe
df['D_before_deg'] = [d for d,i in pre_dirs]
df['I_before_deg'] = [i for d,i in pre_dirs]
df['D_tiltcorr_deg'] = [d for d,i in corrected_dirs]
df['I_tiltcorr_deg'] = [i for d,i in corrected_dirs]
# compute the mean directions (vectorial) before and after and angular
distances to modern mean (D=350.1, I=63.3)
def mean dir from list(D list, I list):
         vs = np.array([dir_to_vector(D,I) for D,I in zip(D_list, I_list)])
         vmean = vs.mean(axis=0)
         R = np.linalg.norm(vmean)
```



```
Dm, Im = vector to dir(vmean)
    return Dm, Im, R
mean before = mean dir from list(df['D before deg'], df['I before deg'])
mean_after = mean_dir_from_list(df['D_tiltcorr_deg'],
df['I tiltcorr deg'])
def angular_distance_deg(u, v):
    u = np.array(u); v = np.array(v)
    cosang = np.dot(u, v) / (np.linalg.norm(u) * np.linalg.norm(v))
    cosang = np.clip(cosang, -1.0, 1.0)
    return rad2deg(np.arccos(cosang))
ang before modern = angular distance deg(vmean before, v modern)
ang_after_modern = angular_distance_deg(vmean_after, v_modern)
# display table
display_df =
df[['sample','strike_deg','dip_deg','D_before_deg','I_before_deg','D_tiltco
rr_deg','I_tiltcorr_deg','NRM']].copy()
display_df =
display df.round({'strike deg':0,'dip deg':0,'D before deg':2,'I before deg
':2, 'D_tiltcorr_deg':2, 'I_tiltcorr_deg':2, 'NRM':2})
import caas_jupyter_tools as cjt
cjt.display dataframe to user("Tilt-correction results (Nongalbibra
samples)", display df)
print("Mean direction (before tilt-correction): D = {:.2f}°, I = {:.2f}°,
resultant length R = {:.3f}".format(*mean_before))
print("Mean direction (after tilt-correction): D = {:.2f}°, I = {:.2f}°,
resultant length R = {:.3f}".format(*mean after))
print("Angular distance between mean (before) and modern field ({:.1f}°,
{:.1f}°): {:.2f}°".format(modern_D, modern_I, ang_before_modern))
print("Angular distance between mean (after) and modern field ({:..1f}°,
{:.1f}°): {:.2f}°".format(modern_D, modern_I, ang_after_modern))
```